



## Flexural Behavior of RC Continuous Beams Strengthened by Cementitious Composite Materials

Hamdy M. Afefy<sup>1,2</sup> , Ashraf M. Heniegal<sup>3</sup> , Ahmed T. Baraghith<sup>1</sup> ,  
Omar M. O. Ibrahim<sup>4</sup> , Mostafa E. A. Eldwiny<sup>5\*</sup>

<sup>1</sup> Department of Structural Engineering, Faculty of Engineering, Tanta University, Tanta, Egypt.

<sup>2</sup> Construction Engineering and Management Department, Faculty of Engineering, Pharos University, Alexandria, Egypt.

<sup>3</sup> Department of Civil Engineering, Faculty of Engineering, Suez University, Suez, 41522, Egypt.

<sup>4</sup> Civil and Architectural Constructions Department, Faculty of Technology and Education, Suez University, P.O. Box: 43221, Suez, Egypt.

<sup>5</sup> Department of Civil Constructions, Beni-Suef University, Beni Suef, Egypt.

Received 30 May 2024; Revised 21 August 2024; Accepted 26 August 2024; Published 01 September 2024

### Abstract

Due to their great strain capacity, high tensile strength, and ability to localize cracks, cementitious composite materials are beneficial for strengthening reinforced concrete (RC) members. This paper illustrates the application of cementitious composite materials in the form of precast thin layers to strengthen a double-spanned, full-scale RC beam. Both positive and negative zones were strengthened by the precast layer embedded into the concrete cover. The precast layers have a dimension of 20 mm in thickness and 150 mm in width as that of the substrate beam and were applied by two configurations: plain and reinforced layers. A ductile smooth steel sheet with 2 mm in thickness and 100 mm in width was used inside the reinforced precast layer. The composite action of the precast layer has mutual benefits; the embedded steel sheet localizes the cracks, while the surrounding cementitious composite materials protect the steel sheet from environmental impact. The experimental results showed that the strengthening system has a significant contribution to improve the failure mode and load-carrying capacity. The use of a plain precast layer caused a 6% increase in the ultimate load and a 33% enhancement in the moment redistribution ratio compared to the control beam (CB). Applying the strengthening system with reinforced precast layer shifted the failure mode from rupture failure in the precast layer to delamination without slippage in the embedded steel sheet and matrix, leading to the full tensile capacity of the precast layer. Besides, the yielded and ultimate loads increased by 34% and 41%, respectively, and maximum deflection increased by 36%. In addition, the beam's ductility increased by 36%, and the moment redistribution ratio was enhanced by 49% compared to the CB.

**Keywords:** Continuous RC Beams; Cementitious Composite Materials; Moment Redistribution; Precast Layer.

## 1. Introduction

RC elements can become more defective during their service life because of mechanical deterioration owing to concrete carbonation, reinforcement corrosion, fires, overloading, etc. Strengthening of RC elements is essential to restore the ultimate capacity and satisfy serviceability limits. In most defective structures, strengthening is more economical to avoid replacing existing structures [1–3]. Numerous studies are focused on strengthening RC beams with a simple span, but a few have studied multi-span RC beams [4, 5]. The flexural capacity of simply supported RC beams

\* Corresponding author: [mostafa.elsaeed@techedu.bsu.edu.eg](mailto:mostafa.elsaeed@techedu.bsu.edu.eg)

<http://dx.doi.org/10.28991/CEJ-2024-010-09-05>



© 2024 by the authors. Licensee C.E.J, Tehran, Iran. This article is an open access article distributed under the terms and conditions of the Creative Commons Attribution (CC-BY) license (<http://creativecommons.org/licenses/by/4.0/>).

depends on the midspan section capacity, whereas continuously supported RC beams depend on the capacities of both positive and negative sections [6-8]. RC continuous beams are widely used in construction sites and are preferred for uniform girders in structural systems that are exposed to seismic hazards. Other benefits of using continuous beams are enhancement of the structure's rigidity and redistribution of the bending moments, which refers to the nonlinear behavior and redundancy of the structure [4, 9].

Over the last decades, several techniques have been used for strengthening the RC beams. Section enlargement (concrete jacketing), externally bounded (EB), and unbounded Fiber Reinforced Polymer (FRP) or steel plate. Near Surface Mounted (NSM) and externally prestressed are the most commonly published techniques [10, 11].

Despite the former techniques providing high efficiency in strengthening RC members, several shortcomings still exist. FRP is a very expensive material, and the efficiency of the strengthening action was lost with high temperatures. Moreover, the substrate materials have a lower tensile strength than resins. In addition to dubious durability because of environmental attacks or corrosion in the EB steel plate. As well as the end anchorage systems that are indispensable to prevent premature failure [12]. Unlike the EB technique, a higher yield load and overall capacity, as well as a low implementation cost, characterize the NSM technique. Besides being more beneficial to protect the reinforcement and adhesive material inside the groove from mechanical damage and environmental attack [9, 13, 14]. Susceptibility to failure due to debonding or concrete cover separation is considered a major shortcoming in the NSM technique when using high-tensile stress bars such as glass fiber-reinforced polymer [5, 15, 16].

Organic resin was substituted by cement as an inorganic binder in cementitious composite materials and applied recently as a suitable substitute for conventional strengthening systems. Such materials are characterized by microcracking produced by the micromechanical tailoring of their constituents, which causes a tension-softening phenomenon after the initiation of the cracks and strain-hardening behavior under increasing uniaxial tension [17-19]. Moreover, these materials are demonstrated by their compatibility with the concrete substrate, constructability, high compressive properties, high ductility, high fire resistance, and easy implementation at low and high temperatures [20–22]. Utilizing cementitious composite materials in a variety of civil engineering applications started to be possible at the (JCI 2002 Japan Concrete Institute) [23]. Applying the cementitious composite materials for strengthening the RC members exhibited higher performance at the service and ultimate limit states [7, 24, 25]. Compared to the EB technique, the strengthened sections using cementitious composite materials achieved higher strength and ductility [26].

Recently, authors decided to use embedded reinforcement sandwiched by cementitious composite materials called fabric-reinforced cementitious matrix (FRCM). These composite matrixes are very applicable to strengthening and rehabilitating RC members [27-29]. High improvements in post-cracking stiffness and ultimate tensile resistance make these composite matrixes suitable to improve the behavior of the strengthened members in flexure [30-32]. The main common types of embedded reinforcement are steel mesh reinforcement or steel fibers and mesh of different fibers (glass, basalt, carbon, polyvinyl alcohol, polyethylene, Polyparaphenylene Benzobisoxazole grids) [33-35]. The results showed that, compared with the normal concrete beam, the stiffness of the composite beams with a 1.7% volume fraction of polyvinyl alcohol (PVA) fibers increased by 14.7%. Furthermore, those with a 1.7% volume fraction of polyethylene (PE) fibers increased by 26.1%. Steel fibers with volume fractions of 0.6% and 1.0% improved the flexural capacity of the PVA fibers composite beams by at least 8.1% [36].

Several studies applied different cementitious composite materials reinforced by sandwiched fabric layers to strengthen the defected side of RC continuous beams [37–39]. According to the test results, the beams' deflections are significantly reduced by a considerable increase in stiffness throughout the service stage, whereas positive strengthening is more obvious after steel yield. The yielding load and ultimate capacity increased by increasing the fabric layers, and the failure mode shifted from fabric sliding to separation from the concrete cover. The end anchorage was very important for large numbers of fabric layers. Higher capacities, more ductile failure, and separation are delayed by using U-shaped wrapping. Others used the Engineered Cementitious Composites material as a transition layer between the strengthening beam and the externally bonded steel or CFRP sheets [40, 41].

This study aims to develop a new technique to cover shortcomings in the common strengthening techniques, such as premature failure due to peeling off or debonding in addition to dubious durability because of environmental attacks or corrosion. As well as the urgency of using the end anchorage systems. The results of the tested beams are compared and analyzed in terms of crack distribution, plateau of the load deflection relationship, yielding and ultimate loads, and moment redistribution ratio.

## 2. Material and Methods

Figure 1 shows the flowchart of the research methodology through which the objectives of this study were achieved.

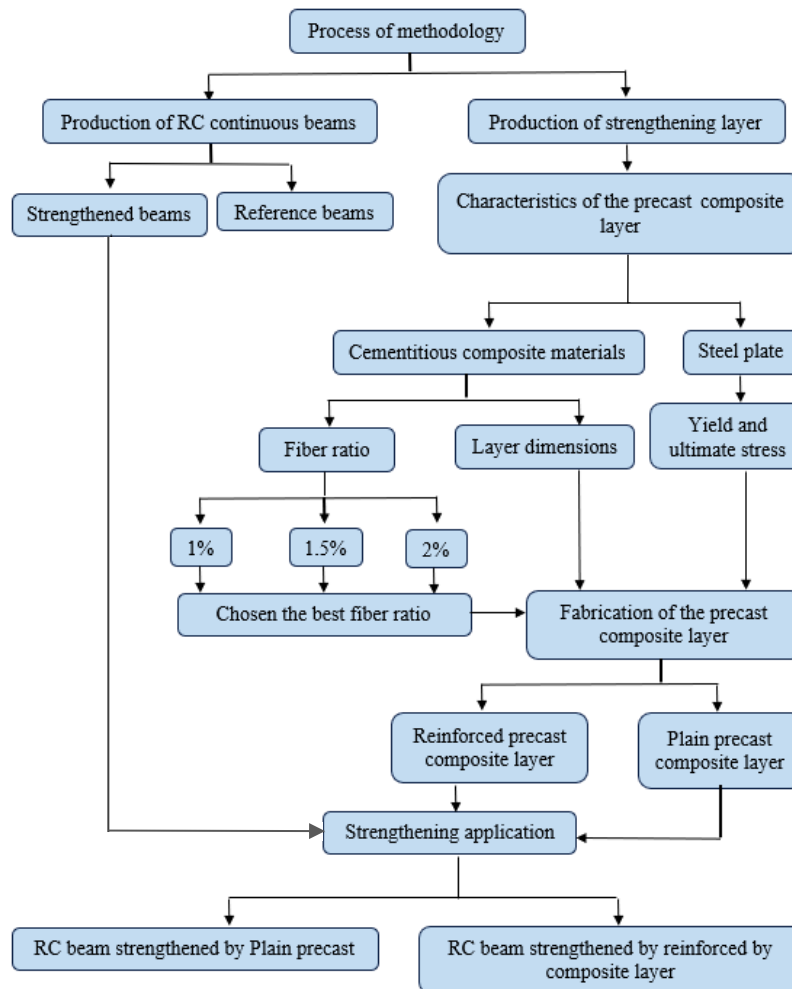


Figure 1. Flowchart for the process of methodology

## 2.1. Material

### 2.1.1. Steel Reinforcement

High-tensile steel (HTS) of 12 mm and 10 mm diameters was used in RC specimens as the main reinforcing steel bars and stirrups, respectively, while the precast layer was reinforced by a smooth steel sheet of normal mild steel (NMS) used as embedded reinforcement in the precast layer. For determining the steel characteristics, three specimens with the same dimensions for each bar's size and steel sheet were tested. The result showed that 412 and 660 MPa are the average yield and ultimate strength, respectively, for main reinforcing bars steel bars as depicted in Figure 2, whereas the average yield and ultimate strength for steel sheet are 310 and 380 MPa, respectively.

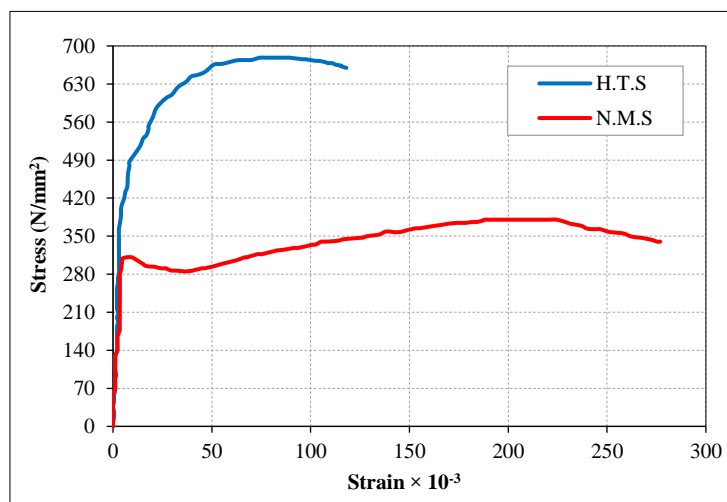


Figure 2. Stress-strain relationships for reinforcing steel bars

### 2.1.2. Concrete

Using ready-mixed concrete, all specimens were cast with a target cylinder compressive strength of 35 MPa. The concrete characteristics were determined using standard cylinders of 300×150 mm and tested by uniaxial compression pre- ASTM C39/C39M-20 [42]. All beams and cylinders were cast and cured in the same conditions. The average results obtained from three cylinders equal 37.2 MPa for compressive strength, 3.71 MPa for indirect tensile strength (splitting tensile tests), 4.2 MPa in the flexural test, and 26800 MPa in the static modulus of elasticity. Table 1 summarizes the concrete mix ingredients per cubic meter.

**Table 1. Mix ingredients for one cubic meter of concrete patch and the cementitious composite layers**

Mix type	W/B*	Cement (kg)	Sand (kg)	Coarse aggregate (kg)	Water (kg)	Silica fume (kg)	Super-plasticizer (kg)	PP Fiber (kg)
RC	0.45	400	530	1280	180	----	----	----
Precast Layer 1% pp Fiber	0.16	1365.32	171.12	---	260	342.1	35.1	8.2
Precast Layer 1.5% pp Fiber	0.16	1365.32	171.12	---	260	342.1	35.1	12.3
Precast Layer 2% pp Fiber	0.16	1365.32	171.12	---	260	342.1	35.1	16.4

\*W/B = water-to-binder ratio, binder = cement + silica fume

### 2.1.3. Precast Composites Layer

The precast layer was made from cementitious composite materials, which consisted of water, ordinary Portland cement, silica fume, fine quartz sand with a diameter less than 0.5 mm, high-range water reducing, and Polypropylene (PP) fibers with a 0.025 mm diameter and 12 mm length. Fibers were added to the matrix by different volume fractions, namely, 1%, 1.5%, and 2.0%, in order to obtain the best ratio of the fibers. The silica fume was used to replace 25% of the design cement. Table 1 summarizes the mix ingredients for one cubic meter of cementitious composite layers. For different volume fractions, the compressive properties of cementitious composite materials were determined by four standard cylinders of 50×100 mm, while the tensile properties were determined according to ASTM A770/A770M-03 [43] using three standard specimens of 50×150 mm with an overall length of 900 mm.

Figure 3 depicts the properties of cementitious composite materials under both compressive and tensile testing. The results demonstrated that the mix with a 2% volume fraction of fiber provides the highest strength in compressive and direct tensile tests, as well as strain hardening behavior, which was quite obvious when compared to the 1 and 1.5% volume fractions of fiber. So, the mix having a 2% fiber volumetric fraction was used in the experimental program to cast the strengthening layers. The first crack is seen in the tested specimens with a 2% volume percentage of fiber at 3.8 MPa, whereas the average compressive and tensile strengths are 69.7 MPa and 6.95 MPa, respectively.

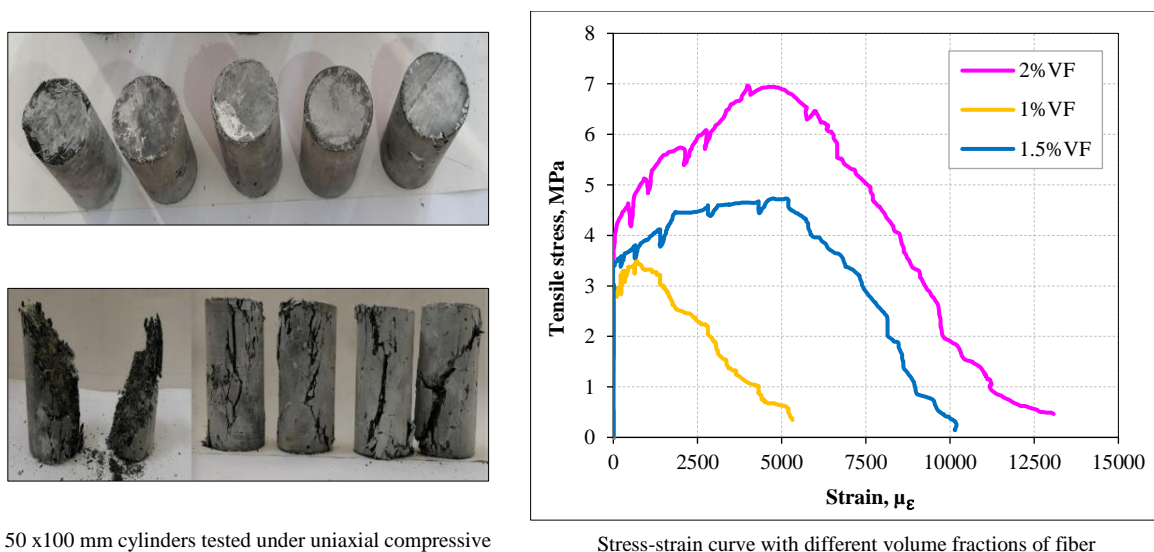


**Figure 3. Properties of cementitious composite materials**

### 2.1.4. Epoxy Adhesive Characteristics

The adhesive material is high-strength epoxy; after complete hardening, the compressive and tensile strengths are 82 and 28 MPa, respectively, while the elastic modulus is 4.8 GPa.

### 2.2. Specimen Detail

The experimental test program consisted of constructing and testing four statically indeterminate RC two-equal spans beams. Two un-strengthened beams served as control beams (CB), and two strengthened beams B1 and B2. All the tested beams had the same concrete dimensions; 150 mm in breadth, 300 mm in depth, and 6000 mm of overall length were divided into two spans of equal length having center-to-center span of 2850 mm. The longitudinal reinforcement for all tested beams is two bars per side with a diameter of 12 mm, whereas the shear reinforcement is closed stirrups with a diameter of 10 mm distributed at 100 mm spacing. The strengthening system consists of precast layer made from cementitious composite materials were applied to cover both positive and negative bending moment regions. The precast layer has 20 mm thickness (as alternative to concrete cover) and 150 mm width (equal to the beam's width). The precast layers in beam "B1" were used in the form of plain type without any reinforcement. The precast layer in beam "B2" was reinforced by an embedded ductile smooth steel sheet extended along the entire strip of 2mm thickness and 100mm breadth.

The ACI PRC-440.2-17 [44] recommended to terminating the strengthening length beyond the inflection point by a half of the effective depth, or at least at 150 mm. In the current study, the negative and positive strengthening lengths in the strengthened beams were designed to cover the zero elastic moment and terminate after it by 225 mm to avoid premature failure, while the positive strengthening length has been started without any anchorage systems. Figure 4 presents the specimens' dimensions, layout of steel reinforcement, loading arrangement, and details of the strengthening system.

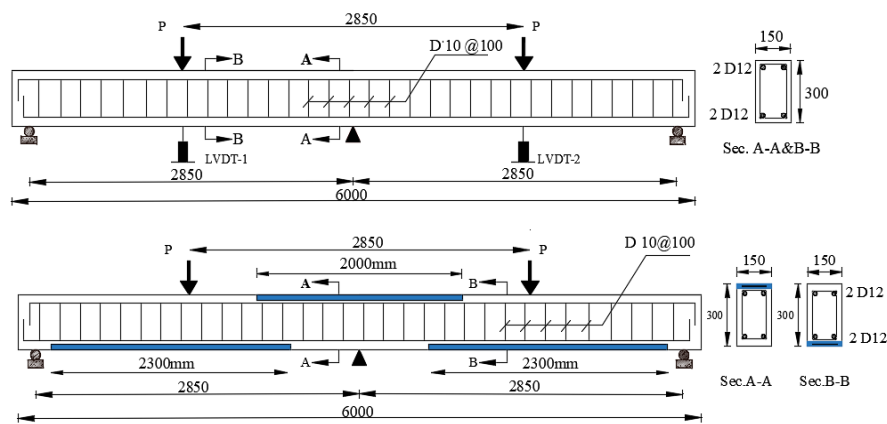


Figure 4. Details of the tested beams and strengthening system

### 2.3. Fabrication of the Precast Layer

The precast layers were cast in a horizontal wooden formwork with a 20mm thickness, 150mm width, and two different lengths of 2000 mm and 2300 mm to be accommodated in the negative and positive bending moment zones, respectively. To ensure good adhesion between the precast layer and the epoxy, the upper surfaces of the layer were not leveled to obtain rough surface. After 24 hours of casting, the precast layers were de-molded and cured for two weeks in a wet condition and then allowed to air dry, refer to Figure 5.



Casting the cementitious composite materials    Composite plate after hardening (Plain)    Composite plate after hardening (Strengthened)

Figure 5. Fabrication of the precast layers

## 2.4. Strengthening Application

The precast layers were applied on substrate RC beams as follows: first, according to the pre-assigned positions of the strengthening length, remove the concrete cover by 21 mm in depth above the main steel at the critical flexural sections by the complete width, as illustrated in Figure 6. Second, epoxy adhesive with another 1 mm thickness was distributed on the concrete surface. Third, epoxy adhesive with another 1 mm thickness was distributed on the unlevelled face of the precast layer, and then the layer was pressed firmly in the groove to reduce any air voids. Finally, the precast layer holds on to the beam faces using steel clamps until it is completely hardened. According to the manufactured epoxy adhesive, it will reach full hardness after five days of application. The strengthened beam was tested after ten days of the strengthening process.



Remove and clean the concrete cover      Application of the epoxy adhesive

Figure 6. Application of precast layers

## 3. Test setup and Instrumentation

Figure 7 shows the test set up and different instruments that were used for collecting data and responses about effectiveness of the studied technique for strengthening two span RC beams. Using a scheme of one static load distributed for two concentrated loads fixed at the midpoint of each span and three supports, all specimens were loaded incrementally up to complete failure. The hydraulic jack has a capacity of 800 kN and 0.4 kN/s average loading rate until failure occurs. The end supports were rested over knife-edge steel, while the central support was rested over a load cell with a capacity of 800 kN in order to measure the intermediate reaction. The total applied load during the testing time was measured using a load cell with a 1400 kN capacity attached under the jack. The vertical displacement in each midspan was measured using LVDTs having 100 mm measuring length. The developed normal strain on was measured using electrical strain gauges attached to the main reinforcing steel bars and steel sheet at the critical section. Ten strain gauges from S1 to S10 were distributed on the positive and negative steel sheets to measure the distribution of developed strain along the entire precast reinforced plates with loading as depicted in Figure 8. The vertical displacement for each part and the normal steel strain along the measuring points, as well as the jack and central support loads, were recorded and stored using a data logger unit (TDS-150).



Figure 7. Test setup and loading arrangement

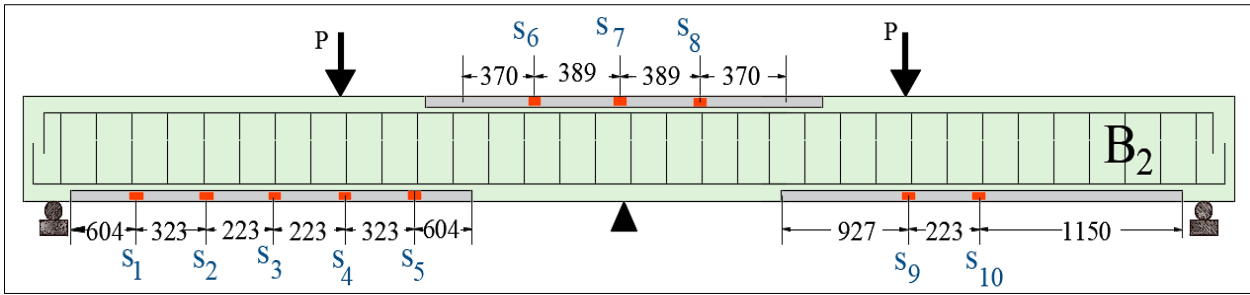


Figure 8. Distribution of the strain gauges along the embedded steel sheet

### 4. Experimental Results

The following sections illustrate the results of tested beams in regard to the energy absorption capacity, cracking pattern, load-deflection behavior, failure mode, ultimate capacity, beam ductility, load-strain response and moment redistribution. The comparison between the control and strengthened beams was calculated according to the following Equations:

$$\text{Decreasing (\%)} = \frac{x_c - x_e}{x_c} \tag{1}$$

$$\text{Increasing (\%)} = \frac{x_e - x_c}{x_c} \tag{2}$$

where  $x_c$  and  $x_e$  are the recorded results for control and strengthened beams, respectively. In the current research work, two control beams (CBs) with the same details were tested to check the test setup. The results display similar behavior for the two CBs, as shown in Figure 9, so the results were compared with one CB and neglected the other.

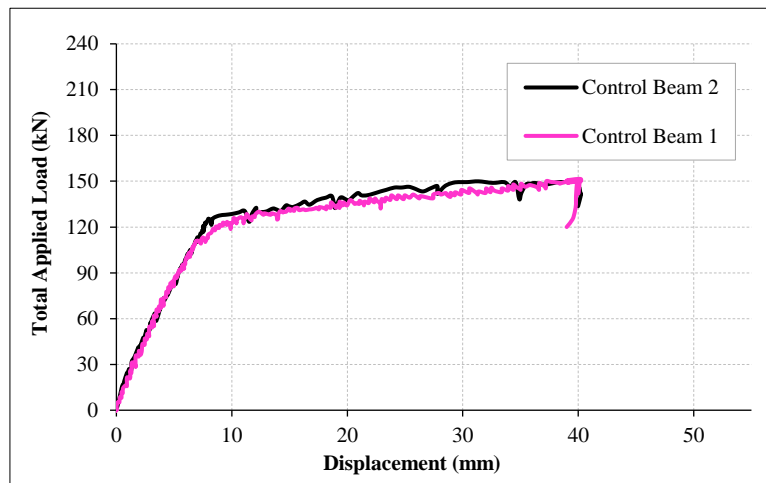


Figure 9. Total applied load vs. mid-span deflection response for control beams

#### 4.1. Load-Deflection Response

The relationships between the total applied load ( $P_t$ ) and the measured deflection ( $\delta$ ) under the concentrated loads were obtained from Jack load, and LVDT1 & LVDT2 are shown in Figure 10. During the loading process, four distinct stages were observed in the load-deflection curves: two stages pre-yielding, named elastic stage (0–1) and concrete cracking stage (1–2), and the other two stages post-yielding, named ultimate stage (2–3) and failure stage (3–4).

According to Figure 10, a marginal contribution to improvement was observed in the strengthened beam behaviour before the initial crack. The load resistance of the strengthened beams showed a significant improvement after the occurrence of concrete cracking and before the main steel started to yield; this is because of the improved tensile resistance of the precast composite layer. While a slight increase in the beam load after the main steel yielded, up to the peak load higher than the CB for B1. Before and after the main steel yielded, the stiffness of the strengthened beams was greater than that of the CB. At a service load corresponding to 0.6 of the ultimate loads and a second steel yielded, the strengthened beams (B1 and B2) showed an average 20% and 65% improvement in the tangent stiffness, respectively. At the pre-yielding stage, the strengthened beams showed a smaller deflection; for instance, at the service stage of about 0.6 from the CB ultimate load, the CB showed a deflection of 5.44 mm, Whereas the strengthened beams B1 and B2 showed deflections of 4.7 mm and 3.37 mm, i.e., 14% and 38% decreasing than the control beam respectively, refer to

Figure 11. After yielding of the tensile steel, a flat plateau without a sharp decline in the loads was observed for the strengthened beams; this means that there isn't any premature failure due to deboning between the steel sheet and the mortar that surrounds it. Generally, these results proved that the precast layer served as additional reinforcement on the tension side and enhanced the flexural behaviour by reducing stiffness loss. Strengthening the RC beams using plain precast thin layer does not have noticeable effect for reducing the ultimate deflection where the ultimate deflection was increased by reinforcing the precast layer using embedded steel sheet.

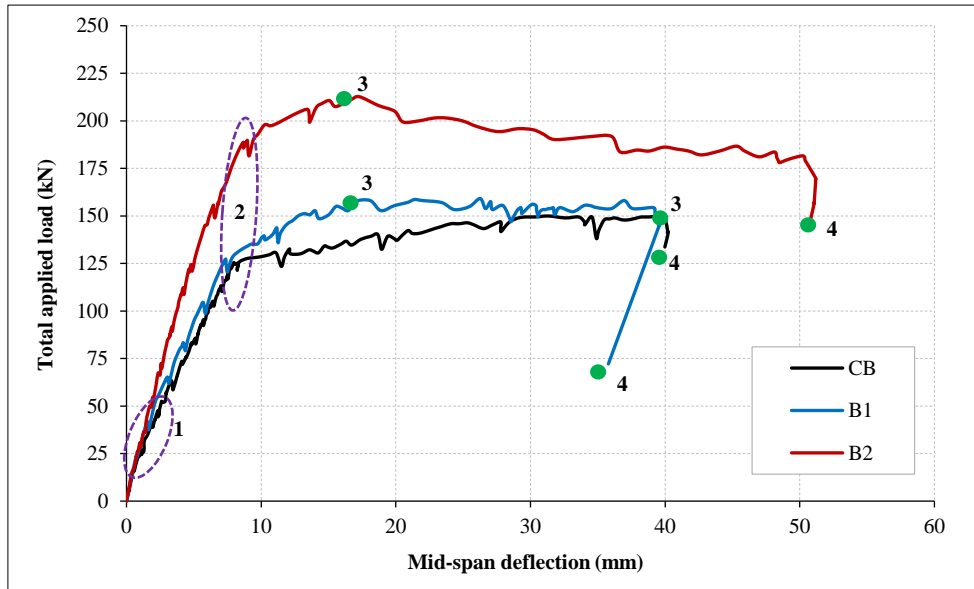


Figure 10. Total applied load vs. midspan-deflection

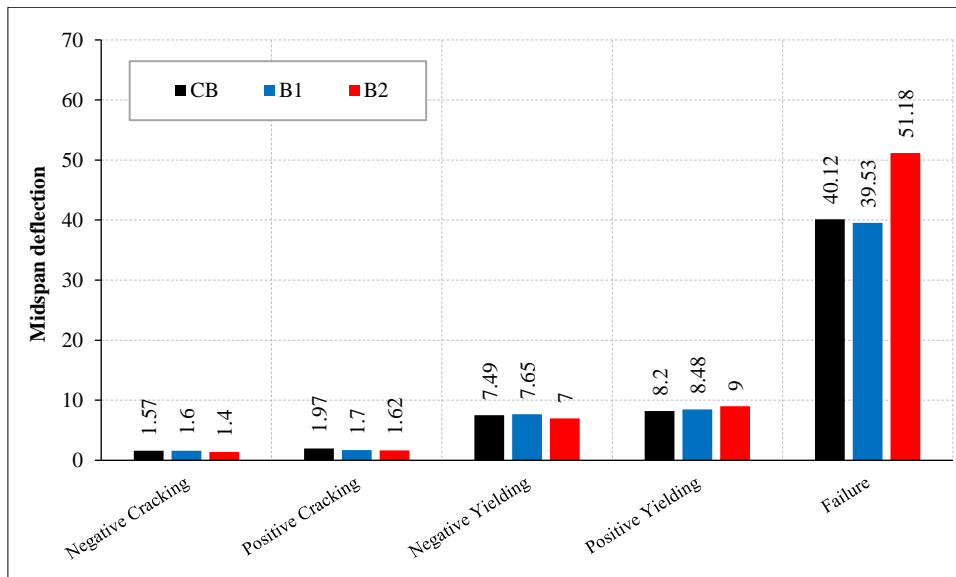


Figure 11. Deflection values at different loading stages

#### 4.2. Energy Absorption Capacity and Failure Modes

According to Hanoon et al. (2017) [45], the energy absorption ( $E_a$ ) for the RC member is considered indicative of structural integrity, and a sign refers to changes in mechanical energy to internal potential energy. The  $E_a$  capacity is defined by the area under the (Pt-  $\delta$ ) until peak load. The main observation was that strengthening RC continuous beams using a precast cementitious composite layer with sufficient development length did not improve their capacity to absorb energy. Applying the strengthening system by precast plain layer showed a lower energy absorption capacity than the CB. This is because of lower resistance of the precast plate after the occurrence of wide cracks in the plate as a result of ruptured in the reinforcement fibres. Despite the embedded steel sheet increased the ultimate load, the ( $E_a$ ) was decreased this is because of the occurrence horizontal shear between the embedded steel sheet and surrounding mortar which led to sharp decline in the load deflection curve. According to the calculations  $E_a$  capacity of the CB is 5100 kN.mm, while it is decreased by about 23% (3900 kN.mm) for B1 and decreased by about 41.8% (2970 kN.mm) for B2.

### 4.3. Failure Mode and Overall Capacity

The maximum mid-span deflection, yield, and overall capacity were determined from the ( $P_t-\delta$ ) relationship and normalized to the CB beam. The yielding load of tension steel at the central support was accurately determined according to the strain gauge measurement. The CB beam failed due to reaching both the main steel and concrete to yield load and maximum compressive resistance, respectively (conventional ductile failure). As illustrated and discussed in reinforcement strains for CB, the negative tension steel yielded at ( $P_y = 121 \text{ kN} = 80\%$  of the ultimate load). Followed by midspan reinforcement yielded ( $P_y = 125 \text{ kN} = 83\%$  of the ultimate load) the beam resistance increased until reaching the peak load ( $P_u = 150.45 \text{ kN}$ ), then the load decreased until the maximum vertical deflection ( $\delta_u = 40.2 \text{ mm}$ ), refer to Figure 12.

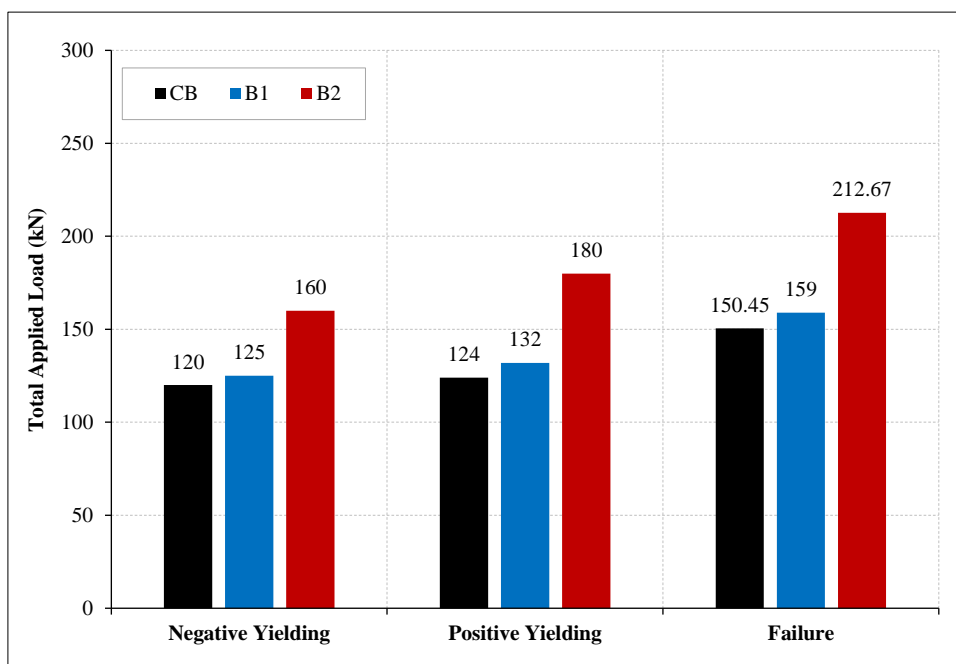


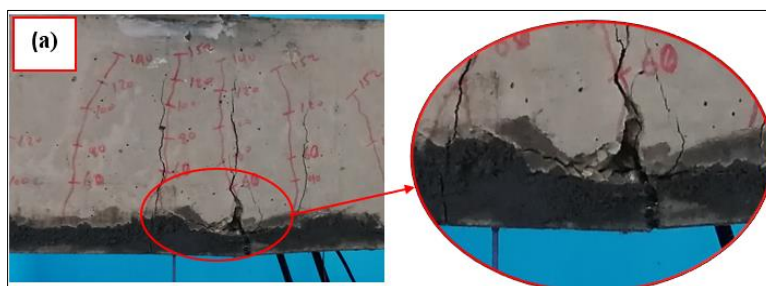
Figure 12. Load values at different loading stages

In comparison with CB beam, the strengthened beam failed according to the following sequence: a) formation of multi-cracks in the precast layer; b) yielding of the embedded steel sheet and tension steel; c) the plastic hinge was formed at the central support and midspan; and d) rupture in the cementitious composite matrix.

The following sections included the modes of failure of the strengthened beams.

- **Rupturing in the precast layer:**

This mode of failure was observed in beam B1. It was generally noticed that using precast layer without embedded reinforcing had lower crack numbers distributed over a small distance. The failure sequence is the formation of cracks in the tension sides until reaching the maximum tension resistance. The major crack crossed the precast plate section once the precast plate ruptured. The stresses are resisted by the main steel only once the main steel reaches the ultimate capacity the beam the beam failed, refer to Figure 13. The negative tension steel in B1 yielded at ( $P_y = 125 \text{ kN} = 81\%$  of the ultimate capacity) and a 5% increase compared to the CB, followed by tension steel yielded at midspan ( $P_y = 132 \text{ kN} = 86\%$  of the ultimate capacity) and a 6% increase compared to the CB. The beam resistance still increases until the failure load ( $P_u = 159 \text{ kN}$ ), a 6% increase, then the load decreased until the maximum vertical deflection at the beam failure ( $\delta_u = 39 \text{ mm}$ ) 3% decreased compared to the CB, refer to Figure 11.





yielded the crack width was suddenly increased by the formation of the plastic hinges. From the zero load until the prior yielding of the steel sheet, the cracks did not cross the precast layer thickness. After the steel sheet yielded, flexural cracks started to occur in the precast layers at maximum positive and negative bending moments. The first crack in B1 appeared in negative side at 38 kN, whereas the first crack appeared in the positive side was at 44 kN, whereas the first negative crack at 40 kN for B2 appeared in the negative side followed by the appearance of the first crack at 45 kN for the positive side. By increasing the beam resistance, the quantity of cracks noticeably increased and wider vertical cracks distributed along the beam sides started appearing in the precast layer and extending toward the strengthening layer's ends until the formation of the plastic hinges. The plastic hinges for B1 started to appear in both negative and positive regions at 127 and 137 kN. Respectively. Whereas the plastic hinges formed at 160 kN in the negative zone followed by the positive region at 180 kN for B2. Generally, at the same load level, strengthened beams exhibited a lower crack width than the control beam as well as the use of embedded steel sheet in the precast layer exhibited arresting to the crack width resulted in smaller crack width lower than the control CB and B1, refer to Figure 16. Figures 17 to 19 show the cracking patterns for control and strengthened beams at failure. By increasing the beam resistance, the cracks were deployed and widened, moreover more cracks started in the flexural zones along the beam's length. Besides, these cracks extended in the direction of central supports and loading points followed by limited concrete crushing at the loading points. The cracking maps for the tested beams at failure were plotted in Figure 20. The rupture in the plain precast plate in B1 results to a limited increase in the crack number as well as wider cracks than the B2. Reinforcing the precast plate using embedded steel sheet ensured a good bond between the steel sheet and the surrounding matrix resulting in good distribution of the cracks along the precast layer at long distance and a larger crack number.

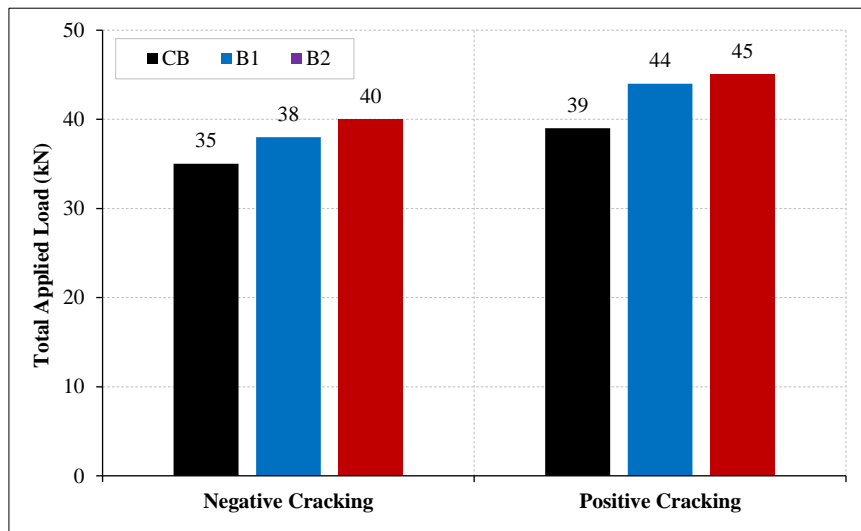


Figure 15. Cracking load in the positive and negative regions

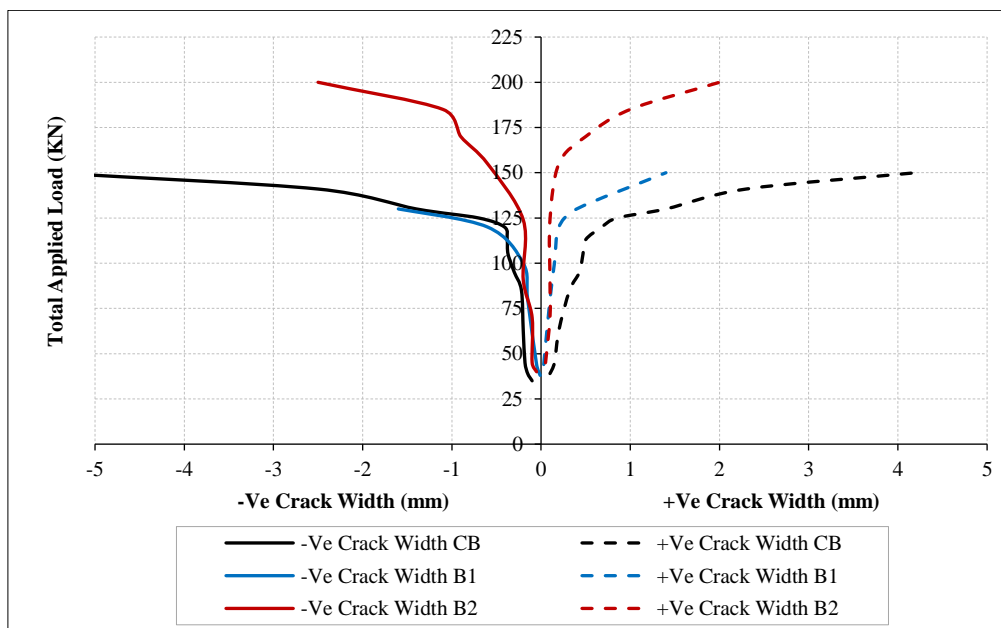


Figure 16. Total applied load vs. crack width

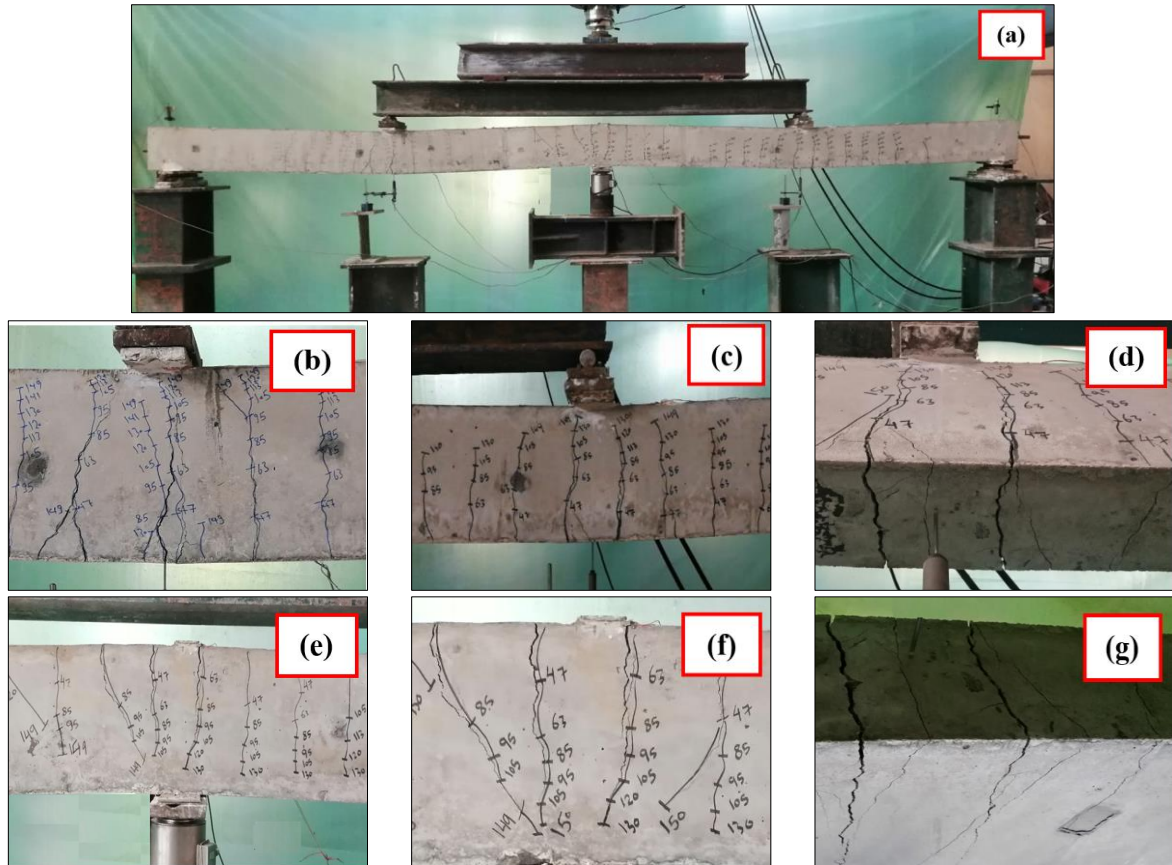


Figure 17. Cracking patterns for CB: (a) Full view; (b) Side view at left span; (c) Side view at right span; (d) Beam soffit at left span; (e and f) Side view at central support and (g) Top view at central support

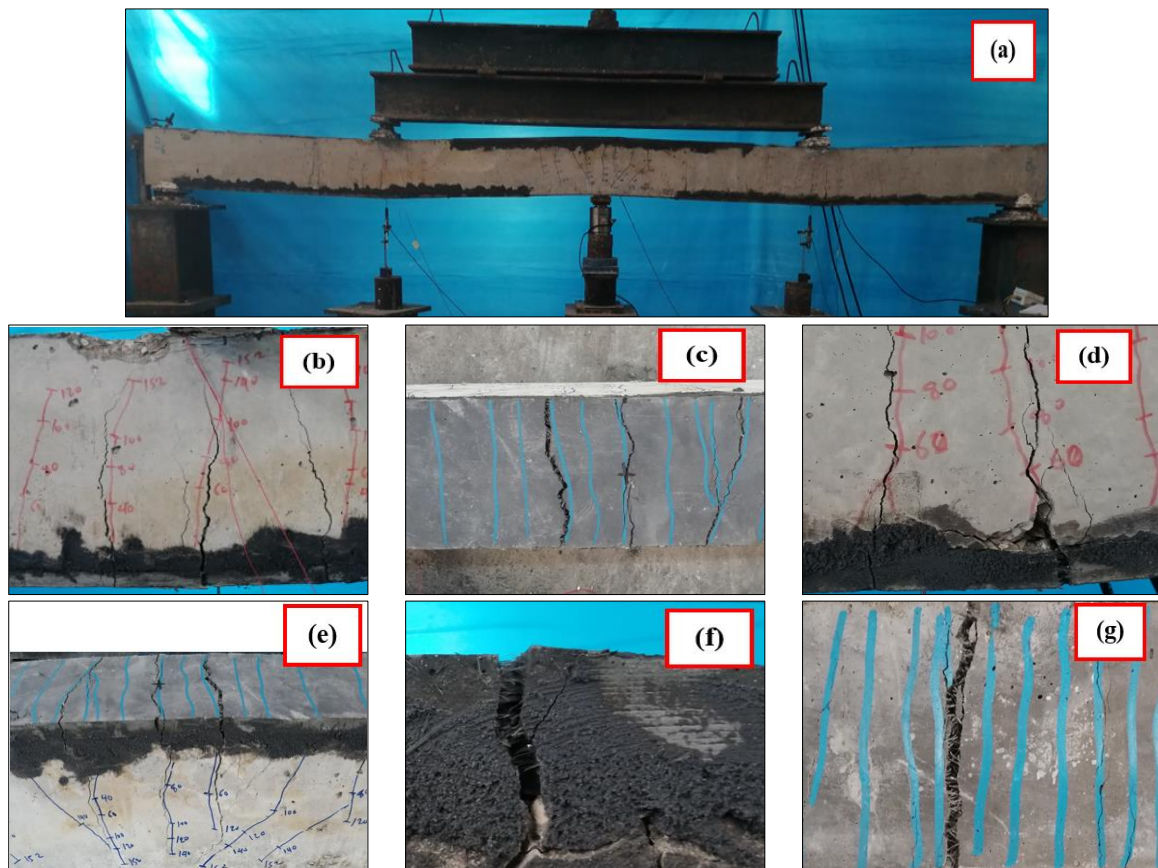


Figure 18. Cracking patterns for B1: (a) Full view; (b) Side view at left span; (c) Bottom view at left span; (d) Bottom view at right span; (e) Side view at central support and (f and g) Rupture at central support

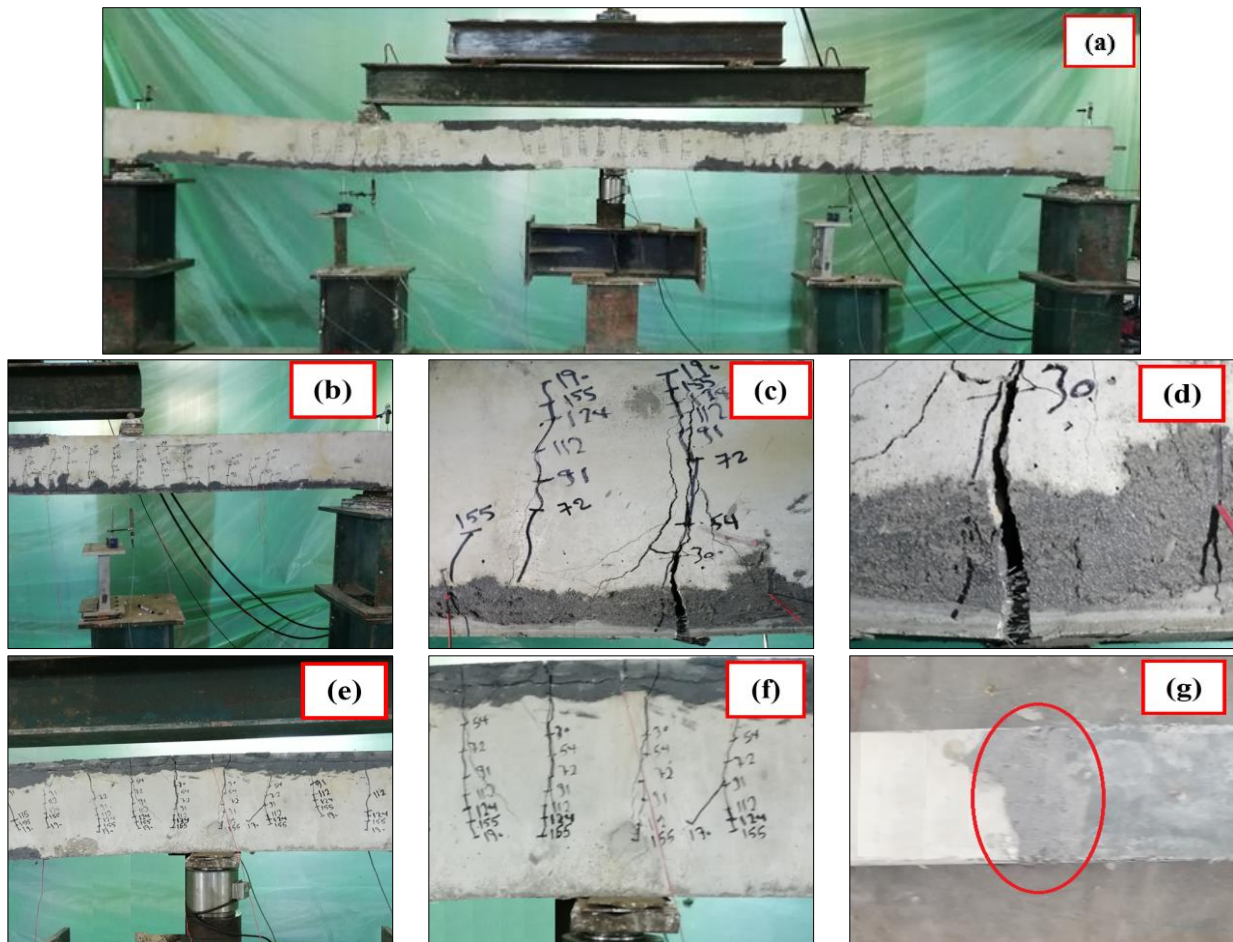


Figure 19. Cracking patterns for B2: (a) Full view; (b and c) Side view at right span; (d) Rupture at right span; (e) Side view at central support; (f) Partial delamination at central support and (g) No slippage at the end

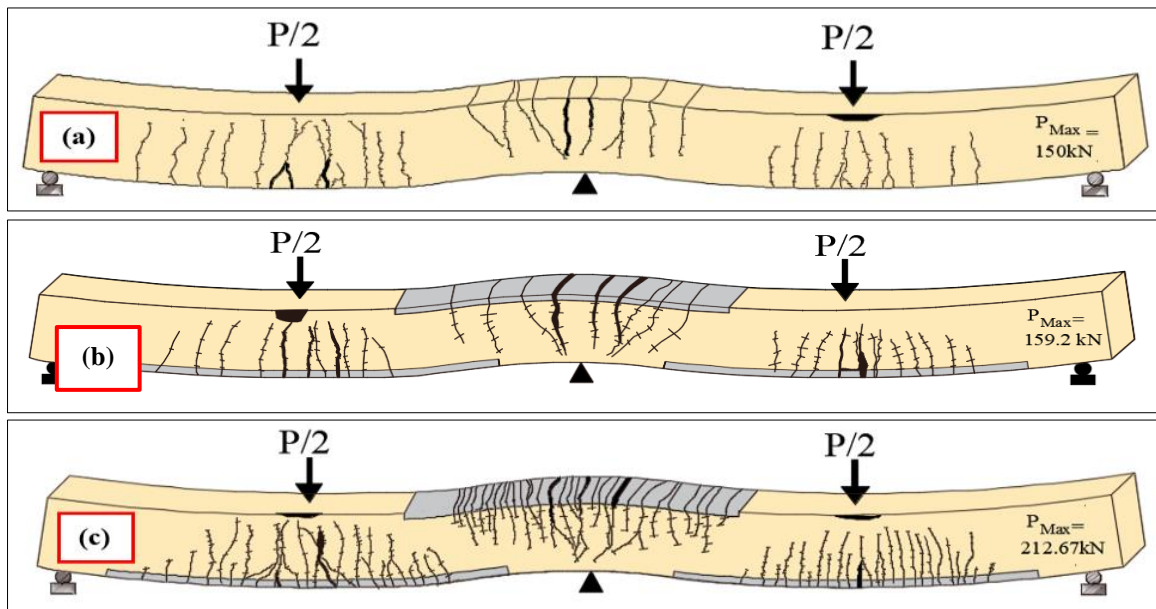


Figure 20. Cracking maps at failure load, (a) CB; (b) B1 and (c) B2

#### 4.5. Beam ductility

According to Mukhopadhyaya et al. (1998) [46], the ductility of RC element tested in flexure was expressed by the ductility index ( $D_I$ ). The  $D_I$  can be calculated according to Equation 3:

$$DI = \frac{\Delta_u}{\Delta_y} \tag{3}$$

where ( $\Delta_u$ ) refers to the recorded midspan displacement at maximum load and ( $\Delta_y$ ) is the recorded midspan displacement at steel yielded, i.e., (the recorded deflection at formation of the last real plastic hinge).

A significant improvement in the measured deflection and load-deflection plateau refers to an enhancement in the ductility index. Applying the strengthening system by plain precast plate showed decreasing in the  $D_I$  by about 11% than the CB. This decreasing is due to brittle resistance of the cementitious composite materials without reinforcement. Whereas the  $D_I$  for B2 increased by about 4.7% which reflects the capability of the precast layer to absorb the energy and exhibit an acceptable level of strain-hardening response. This increase in the ductility index reflects the perfect bond mechanism between the precast layer and the specimen surface.

#### 4.6. Strain Measurements

Strain gauges were mounted on the main reinforcing steel bars and the embedded steel sheets at the critical section zones to trace the strain development along the entire loading plateau.

#### 4.7. Tensile Strains on the Longitudinal Steel Bars

As depicted in Figure 21, similar to the ( $P-\delta$ ) curves, there are three distinguished stages in the load-strain curve, separated by a concrete cracking point and a tensile steel yielding point and influenced by the strengthening system. For the CB, all tensile stresses are carried by the reinforced steel bars after concrete cracking; in contrast, in the strengthened beams, stresses are carried by longitudinal steel bars and the precast composite layers after concrete cracking. The control and strengthened beams achieved similar negative and positive steel strains of almost zero until the first concrete crack due to the slight impact of the precast layer at this stage. As identical and in agreement with the ( $P-\delta$ ) curve, a visible effect of the precast layer in the strengthened beam was observed once the first crack appeared prior to steel yielded. The use of plain precast layer in B1 showed a limited decrease in the main steel strain compared to CB after concrete cracking whereas the yielding load was significantly greater than CB. Reinforcing the precast layer by embedded steel sheet in B2 showed a linear response and decrease in the tensile steel strains compared to the CB and B1 at the same load in negative or positive regions after the cracking initiated. This is due to the large tensile resistance of the precast composite layer, which participated as additional reinforcement. afterward, the steel strain rapidly increased up to failure. The yielding load was significantly greater than CB and B1. These results established the notable contribution of the strengthening system.

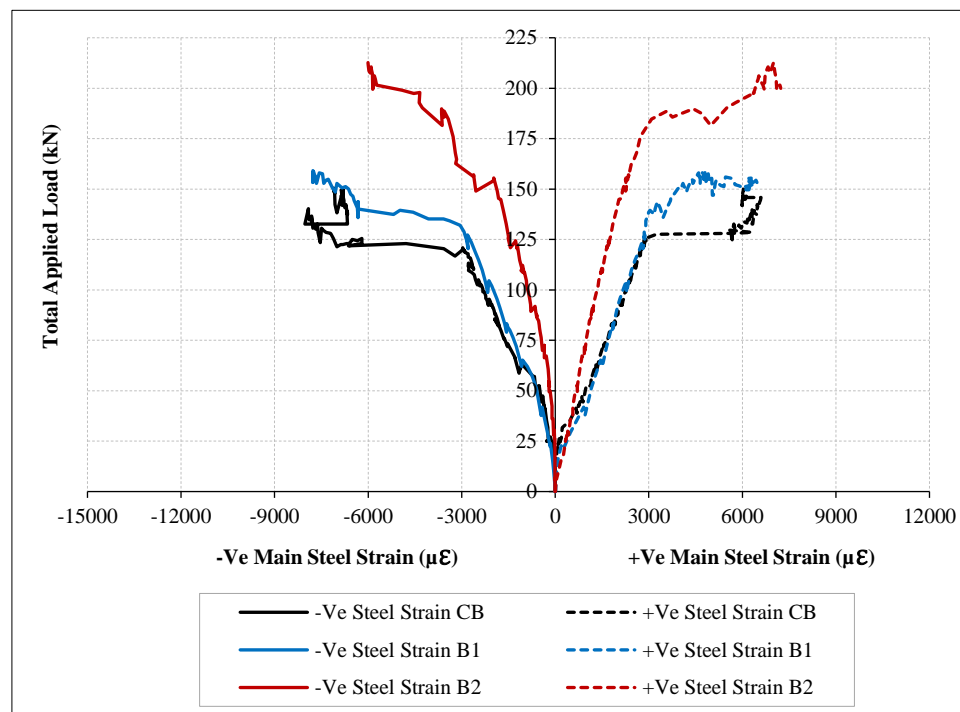


Figure 21. Load vs. main steel strain at the negative and positive regions

#### 4.8. Longitudinal Steel Sheet Strain

The development of the longitudinal normal strains on the embedded steel sheet are shown in Figures 22-a to 22-c. Three strain gauges are located in the negative strengthening layer, whereas five strain gauges are attached to the positive strengthening layer at the left span and two are attached to the right span for more accuracy in the results. Good

distribution of the strain values and the proportionality of the developed values with the location of the maximum stressed section showed good and complete adhesion between the internal steel and the surrounding cementitious materials as well as perfect bond between the strengthening layer and the substrate beam. The highest recorded strain value was exhibited at mid-span and central support sections, while the lowest recorded strain values were at the ends of the composite layer. The left span strains agree with the right span strain, which reflects the accuracy of the test setup and loading points. A linear distribution was observed in the steel sheet strains before the main steel yielded, while the strain gradient increased by increasing the beam resistance until reaching the maximum tensile resistance of the steel sheet, followed by rupture in the cementitious materials. There was no debonding between the steel layer and the surrounding material until the precast layer ruptured. These results proved the visible contribution of the composite precast layer to improving the specimen's behaviour.

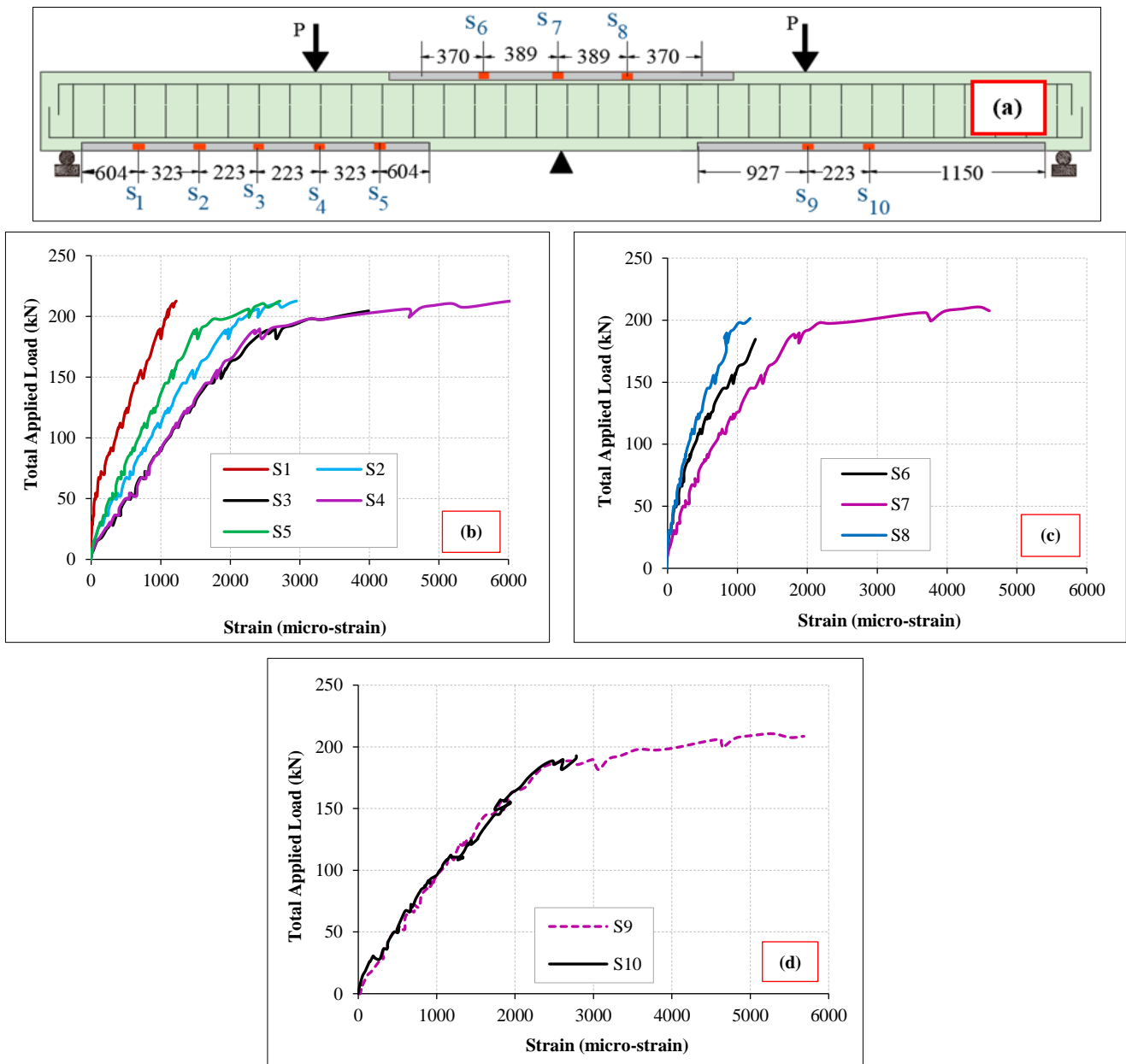


Figure 22. Variation in longitudinal strain along the steel sheet in the strengthened beam: (a) Position of the strain gauges; (b) Strain distribution in the positive steel sheet at left span;(c) Strain distribution in the negative steel sheet (d) Strain distribution in the positive steel sheet at right span.

#### 4.9. Redistributed of Moment Capacity

The moment redistribution capacity reflects the nonlinear behavior of the RC beam and overall structure redundancy. The arrangement and quantity of steel reinforcement and loading type, as well as the support width, all have a noticeable effect on the moment redistribution ratio in RC beams. Several codes allow for a moment redistribution (MR) of 15–

30% between critical sections in continuous concrete beams such as BS EN 1992-1-1:2004 [47] and ACI 318-14 [48]. These codes did not allow the MR to occur in the RC members that were reinforced or strengthened by brittle material such as FRP because it lacks the required level of ductility and has very poor bond conditions.

The jack load at different levels versus the measured support’s reactions in compression with the elastic reaction are plotted in Figures 23. The central reaction was calculated utilizing a load cell placed under the central support, where the end reactions are calculated from equilibrium. The experimental moments along the beam length were calculated using the recorded support’s reaction. The elastic moment was calculated according to Figures 24 by assuming a uniform flexural stiffness along the tested specimens.

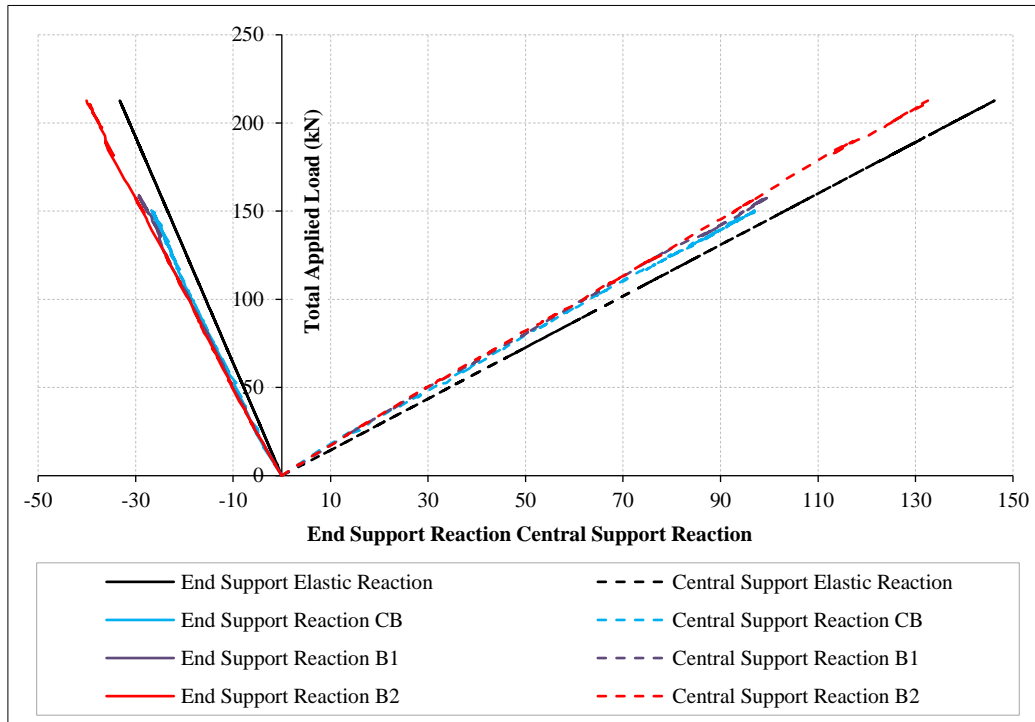


Figure 23. The measured reaction at the end and central supports

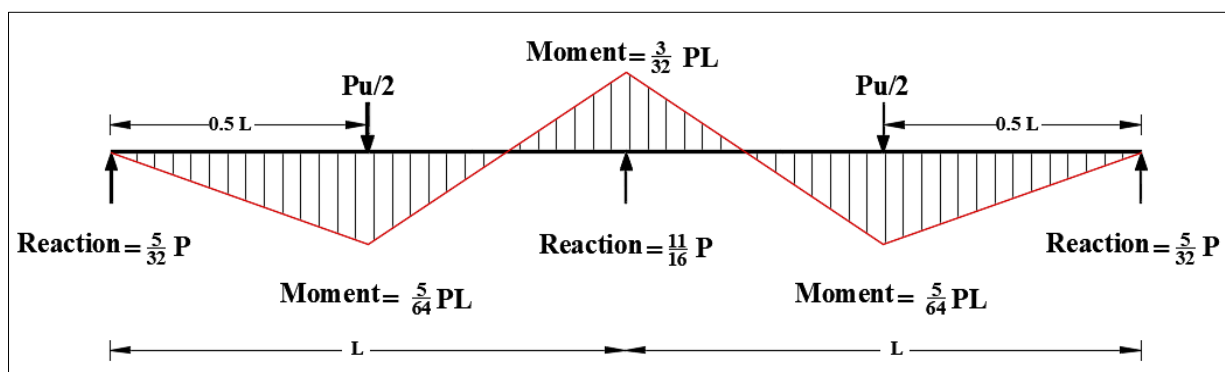


Figure 24. Elastic moment along the tested beam

As depicted in Figure 23, the actual measured reaction at the central support started to decrease lower than the elastic reaction after concrete cracking in both control and strengthened beams. While the decrease at the ultimate load was very clear that indicates that a redistribution of moment occurred. The actual central support reaction for the CB is higher than the strengthened beam at the ultimate load, which indicates the occurrence of a higher moment redistribution level for the strengthened beams than the CB. After concrete cracking, the end reactions increased until the ultimate load, which emphasized the central support reactions. This indicates the redistribution of the moment from the negative to the positive zone as explained in the next section. Table 2 summarizes the experimental results representing the ultimate load ( $P_u$ ), the central support reaction ( $R_c$ ), the end support reaction ( $R_e$ ), and positive and negative elastic bending ( $M_e^{Po}$  &  $M_e^{Ne}$ ), actual positive & negative bending moment ( $M_{ac}^{Po}$  &  $M_{ac}^{Ne}$ ) and moment redistribution ratio ( $\beta$ ).

**Table 2. Experimental measured results at different load levels for the tested beams**

Beam	Pu, kN	Support reaction, kN		+Ve BM, kN.m			-Ve BM, kN.m		
		Rc (1)	Re (2)	$M_e^{Po}$ (3)	$M_{ac}^{Po}$ (4)	%β (5)	$M_e^{Ne}$ (6)	$M_{ac}^{Ne}$ (7)	%β (8)
CB	150.22	96.94	26.75	33.50	38.12	13.8	40.198	30.945	-23
B1	159.12	100.50	29.31	35.43	41.76	17.78	42.51	29.8	-29.78
B2	212.67	132.546	40.062	47.352	57.088	20.56	56.823	37.350	-34.3

- (1) The measured reaction at central support.
- (2) External reaction measured from equilibrium.
- (3) The ultimate elastic positive bending moment was determined by Equation 4.
- (4) The actual positive bending moment at ultimate load was determined by Equation 6.
- (5) The moment redistribution ratio at the positive zone is determined by Equation 8.
- (6) The ultimate elastic negative bending moment was determined by Equation 5.
- (7) The actual negative bending moment at ultimate load was determined by Equation 7.
- (8) The negative redistribution moment ratio is determined by Equation 8.

The elastic positive and negative bending moment  $M_e^{Po}$  &  $M_e^{Ne}$  were calculated according to Equations 4 and 5, while Equations 6 and 7 are used to calculate the actual positive and negative bending moment ( $M_{ac}^{Po}$ ) & ( $M_{ac}^{Ne}$ ). At ultimate load, the moment redistribution ratio ( $\beta$ ) was calculated according to Equation 8. Furthermore, the actual moment compared with the elastic moment at the ultimate load is depicted in Figure 25.

$$M_e^{Po} = \frac{5P_uL}{64} \tag{4}$$

$$M_e^{Ne} = \frac{5P_uL}{64} \tag{5}$$

$$M_{ac}^{Po} = \frac{(P_u - R_C)L}{4} \tag{6}$$

$$M_{ac}^{Ne} = \frac{(P_u - 2R_C)L}{4} \tag{7}$$

$$\beta(\%) = \left[ \frac{M_e - M_{ac}}{M_e} \right] \times 100\% \tag{8}$$

where L= span length.

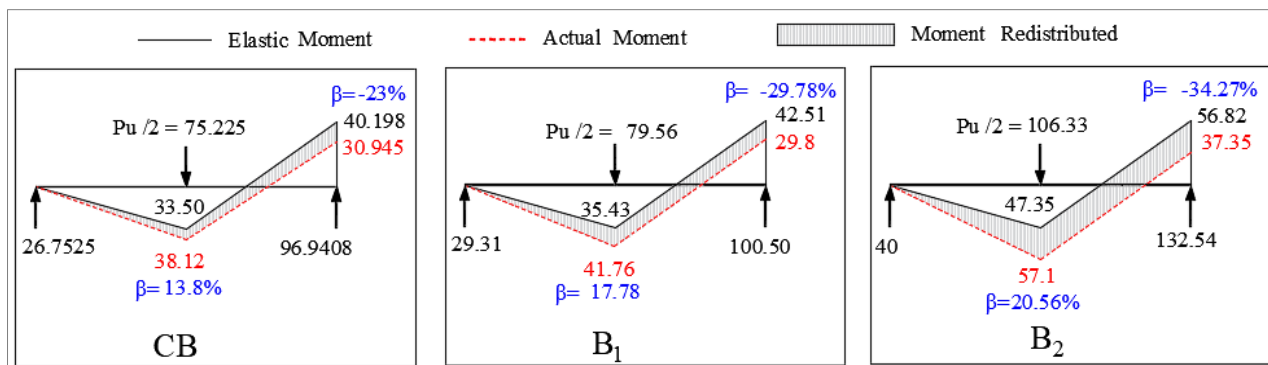


**Figure 25. Elastic and actual moment at the ultimate load (moment in kN.m and loads in kN)**

As depicted in Figure 25 and Table 2, the moment redistributed occurred by migration from the negative to positive regions in both CB and strengthened beams. The moment redistribution ratio ( $\beta$ ) in the CB was equal to -23% in the negative and 13.8% for the positive, whereas the moment redistribution ratio for B1 was equal to -29.78% and 17.78% in the negative and positive zones, respectively, and the moment redistribution ratio for B2 was equal to -34.27% and 20.56% in the negative and positive zones. Compared to the CB, the moment redistribution ratio ( $\beta$ ) was enhanced by about 30% for B1 and 49% for B2.

By comparing those results with other studies that focused on strengthening RC continuous beams using different techniques such as [9, 38, 49-51], a higher level of moment redistribution occurred than in the listed references. These outcomes demonstrate the effectiveness and efficiency of cementitious composite materials in strengthening and repairing the RC beams.

## 5. Conclusion

Based on the results of the experimental program, taking into consideration the adopted concrete dimensions and reinforcement details as well as the dimensions and characteristics of the precast layer, it could be concluded that utilizing the precast composite layer with a 20mm thickness is very effective for strengthening two-span RC beams. This could be attributed to the fact that the strengthening system worked as additional reinforcement on the tension side and caused a significant contribution to improving the cracking arrangement and failure mode by increasing the crack numbers and distribution distance of the strengthened beams without any end anchorage systems. Despite the plain precast layer having a limited contribution to the flexural performance, the moment redistribution ratio was enhanced by about 33%, whereas reinforcing the precast layer by embedded steel sheet showed a 49% increase compared to the control beam.

Respectively for B1 and B2 compared with the CB, the yielded load was enhanced by 5% and 34%, while the ultimate load was enhanced by 6% and 41%. On the other hand, the ductility for the strengthened beam increased by 36% for B2 and decreased by 4% for B1. Besides, reinforcing the precast layer using embedded steel sheet led to changing the mode of failure from rupture in the precast layer to delamination between the precast plate and concrete without premature failure or slippage. A flat plateau without a sharp decline in the load was observed in B2, which indicated that there hasn't been any premature failure owing to peeling off between the concrete and precast layer or debonding between the steel sheet and the surround mortar.

## 6. Declarations

### 6.1. Author Contributions

Conceptualization, H.M.A. and A.T.B.; methodology, H.M.A., A.M.H., A.T.B., O.M.I., and M.E.E.; software, M.E.E.; validation, H.M.A., A.M.H., A.T.B., and M.E.E.; formal analysis, H.M.A., A.T.B., and M.E.E.; investigation, H.M.A., A.M.H., A.T.B., O.M.I., and M.E.E.; resources, O.M.I. and M.E.E.; data curation, A.T.B. and M.E.E.; writing—original draft preparation, H.M.A. and M.E.E.; writing—review and editing, H.M.A. and M.E.E.; visualization, A.T.B. and M.E.E.; supervision, H.M.A. and A.T.B.; project administration, A.T.B. and M.E.E.; funding acquisition, M.E.E. All authors have read and agreed to the published version of the manuscript.

### 6.2. Data Availability Statement

The data presented in this study are available in the article.

### 6.3. Funding

The authors received no financial support for the research, authorship, and/or publication of this article.

### 6.4. Acknowledgements

This work was carried out in the Laboratory of Reinforced Concrete and Heavy-Weight Structures, Faculty of Engineering, Tanta University, Egypt. The authors are thankful to the lab staff for their support and technical assistance in casting and testing specimens. This work is part of the Ph.D. for the fifth author.

### 6.5. Conflicts of Interest

The authors declare no conflict of interest.

## 7. References

- [1] Nordin, H., & Täljsten, B. (2006). Concrete Beams Strengthened with Prestressed Near Surface Mounted CFRP. *Journal of Composites for Construction*, 10(1), 60–68. doi:10.1061/(asce)1090-0268(2006)10:1(60).
- [2] Jumaat, M. Z., Rahman, M. M., & Alam, M. A. (2010). Flexural strengthening of RC continuous T beam using CFRP laminate: A review. *International Journal of Physical Sciences*, 5(6), 619–625.
- [3] Abdelaleem, T., Diab, H. M., & Rashwan, M. M. (2021, December). New aspects about the effect of critical regions reinforcement on the strength and moment redistribution of RC continuous T-beams (Experimental and numerical study). *Structures*, 34, 4834–4850. doi:10.1016/j.istruc.2021.10.065.
- [4] Salama, A. S. D., Hawileh, R. A., & Abdalla, J. A. (2019). Performance of externally strengthened RC beams with side-bonded CFRP sheets. *Composite Structures*, 212, 281–290. doi:10.1016/j.compstruct.2019.01.045.
- [5] Abdallah, M., Al Mahmoud, F., Khelil, A., & Mercier, J. (2021). Efficiency of EB CFRP composites for flexural strengthening of continuous RC beams: A comparative study with NSM CFRP rods. *Structures*, 34, 1567–1588. doi:10.1016/j.istruc.2021.08.073.
- [6] El-Maaddawy, T., Alshawa, J., & El-Ariss, B. (2016). Strengthening of continuous concrete slab strips containing cutouts. *ACI Structural Journal*, 113(6), 1243–1252. doi:10.14359/51689027.

- [7] Alkhalil, J., & El-Maaddawy, T. (2017). Nonlinear Flexural Response of Continuous Concrete Slab Strips Strengthened with Near Surface-Mounted Composites. *Journal of Composites for Construction*, 21(1), 4016071. doi:10.1061/(asce)cc.1943-5614.0000730.
- [8] Su, M. ni, Zeng, C., Li, W. qian, Zhu, J. H., Lin, W. hao, Ueda, T., & Xing, F. (2020). Flexural performance of corroded continuous RC beams rehabilitated by ICCP-SS. *Composite Structures*, 232, 111556. doi:10.1016/j.compstruct.2019.111556.
- [9] Abdallah, M., Al Mahmoud, F., Khelil, A., Mercier, J., & Almassri, B. (2020). Assessment of the flexural behavior of continuous RC beams strengthened with NSM-FRP bars, experimental and analytical study. *Composite Structures*, 242, 112127. doi:10.1016/j.compstruct.2020.112127.
- [10] Hosen, M. A., Jumaat, M. Z., & Islam, A. B. M. S. (2015). Side Near Surface Mounted (SNSM) technique for flexural enhancement of RC beams. *Materials & Design*, 83, 587–597. doi:10.1016/j.matdes.2015.06.035.
- [11] Nayak, A. N., Kumari, A., & Swain, R. B. (2018). Strengthening of RC Beams Using Externally Bonded Fibre Reinforced Polymer Composites. *Structures*, 14, 137–152. doi:10.1016/j.istruc.2018.03.004.
- [12] De Lorenzis, L., & Nanni, A. (2001). Shear strengthening of reinforced concrete beams with near-surface mounted fiber-reinforced polymer rods. *ACI Structural Journal*, 98(1), 60–68. doi:10.14359/10147.
- [13] Hassan, T., & Rizkalla, S. (2003). Investigation of Bond in Concrete Structures Strengthened with Near Surface Mounted Carbon Fiber Reinforced Polymer Strips. *Journal of Composites for Construction*, 7(3), 248–257. doi:10.1061/(asce)1090-0268(2003)7:3(248).
- [14] Dias, S. J. E., Barros, J. A. O., & Janwaen, W. (2018). Behavior of RC beams flexurally strengthened with NSM CFRP laminates. *Composite Structures*, 201, 363–376. doi:10.1016/j.compstruct.2018.05.126.
- [15] Bilotta, A., Ceroni, F., Nigro, E., & Pecce, M. (2015). Efficiency of CFRP NSM strips and EBR plates for flexural strengthening of RC beams and loading pattern influence. *Composite Structures*, 124, 163–175. doi:10.1016/j.compstruct.2014.12.046.
- [16] Al-Mahmoud, F., Castel, A., & Franois, R. (2012). Failure modes and failure mechanisms of RC members strengthened by NSM CFRP composites - Analysis of pull-out failure mode. *Composites Part B: Engineering*, 43(4), 1893–1901. doi:10.1016/j.compositesb.2012.01.020.
- [17] Singh, M., Saini, B., & Chalak, H. D. (2019). Performance and composition analysis of engineered cementitious composite (ECC) – A review. *Journal of Building Engineering*, 26, 100851. doi:10.1016/j.jobe.2019.100851.
- [18] Li, V. C., Wang, S., & Wu, C. (2001). Tensile strain-hardening behavior of polyvinyl alcohol engineered cementitious composite (PVA-ECC). *ACI Materials Journal*, 98(6), 483–492. doi:10.14359/10851.
- [19] Afefy, H. M., Kassem, N., & Hussein, M. (2015). Enhancement of flexural behaviour of CFRP-strengthened reinforced concrete beams using engineered cementitious composites transition layer. *Structure and Infrastructure Engineering*, 11(8), 1042–1053. doi:10.1080/15732479.2014.930497.
- [20] Hussein, M., Kunieda, M., & Nakamura, H. (2012). Strength and ductility of RC beams strengthened with steel-reinforced strain hardening cementitious composites. *Cement and Concrete Composites*, 34(9), 1061–1066. doi:10.1016/j.cemconcomp.2012.06.004.
- [21] Zhang, D., Ueda, T., & Furuuchi, H. (2012). A design proposal for concrete cover separation in beams strengthened by various externally bonded tension reinforcements. *Journal of Advanced Concrete Technology*, 10(9), 285–300. doi:10.3151/jact.10.285.
- [22] Zhang, J., Wang, Z., Ju, X., & Shi, Z. (2014). Simulation of flexural performance of layered ECC-concrete composite beam with fracture mechanics model. *Engineering Fracture Mechanics*, 131, 419–438. doi:10.1016/j.engfracmech.2014.08.016.
- [23] Japan Concrete Institute (JCI). (2002). Proceedings of the JCI international workshop on ductile fiber reinforced cementitious composites (DFRCC), Japan Concrete Institute, Chiyoda-ku, Japan.
- [24] Afefy, H. M. E. D., & Mahmoud, M. H. (2014). Structural performance of RC slabs provided by pre-cast ECC strips in tension cover zone. *Construction and Building Materials*, 65, 103–113. doi:10.1016/j.conbuildmat.2014.04.096.
- [25] Baraghith, A. T., Khalil, A. H. A., Etman, E. E., & Behiry, R. N. (2023). Improving the shear behavior of RC dapped-end beams using precast strain-hardening cementitious composite (P-SHCC) plates. *Structures*, 50, 978–997. doi:10.1016/j.istruc.2023.02.059.
- [26] Afefy, H. M., Baraghith, A. T., & Mahmoud, M. H. (2020). Retrofitting of defected reinforced-concrete cantilever slabs using different techniques. *Magazine of Concrete Research*, 72(14), 703–719. doi:10.1680/jmacr.18.00340.
- [27] Qasim, M., Lee, C. K., & Zhang, Y. X. (2023). Flexural strengthening of reinforced concrete beams using hybrid fibre reinforced engineered cementitious composite. *Engineering Structures*, 284, 115992. doi:10.1016/j.engstruct.2023.115992.
- [28] Tang, T. T., Peng, K. Di, Huang, J. Q., Guo, D., & Huang, B. T. (2024). Flexural performance of reinforced concrete beams strengthened with FRP-reinforced geopolymer matrix: Numerical validation and parametric study. *Advances in Structural Engineering*, 27(2), 269–287. doi:10.1177/13694332231222079.

- [29] ACI PRC-549.4-20. (2020). Guide to Design and Construction of Externally Bonded Fabric-Reinforced and Steel-Reinforced Grout Systems for Repair and Strengthening of Concrete Structures. American Concrete Institute, Michigan, United States.
- [30] Täljsten, B., & Blanksvärd, T. (2007). Mineral-Based Bonding of Carbon FRP to Strengthen Concrete Structures. *Journal of Composites for Construction*, 11(2), 120–128. doi:10.1061/(asce)1090-0268(2007)11:2(120).
- [31] Hashemi, S., & Al-Mahaidi, R. (2012). Experimental and finite element analysis of flexural behavior of FRP-strengthened RC beams using cement-based adhesives. *Construction and Building Materials*, 26(1), 268–273. doi:10.1016/j.conbuildmat.2011.06.021.
- [32] Elsanadedy, H. M., Almusallam, T. H., Alsayed, S. H., & Al-Salloum, Y. A. (2013). Flexural strengthening of RC beams using textile reinforced mortar - Experimental and numerical study. *Composite Structures*, 97, 40–55. doi:10.1016/j.compstruct.2012.09.053.
- [33] Kunieda, M., Hussein, M., Ueda, N., & Nakamura, H. (2010). Enhancement of crack distribution of UHP-SHCC under axial tension using steel reinforcement. *Journal of Advanced Concrete Technology*, 8(1), 49–57. doi:10.3151/jact.8.49.
- [34] Barhum, R., & Mechtcherine, V. (2012). Effect of short, dispersed glass and carbon fibres on the behaviour of textile-reinforced concrete under tensile loading. *Engineering Fracture Mechanics*, 92, 56–71. doi:10.1016/j.engfracmech.2012.06.001.
- [35] Baraghith, A. T., Mansour, W., Behiry, R. N., & Fayed, S. (2022). Effectiveness of SHCC strips reinforced with glass fiber textile mesh layers for shear strengthening of RC beams: Experimental and numerical assessments. *Construction and Building Materials*, 327, 127036. doi:10.1016/j.conbuildmat.2022.127036.
- [36] Wu, F., Zhao, B., Cao, J., Shen, X., Wang, Z., Lei, H., & Cui, Z. (2024). Experimental and theoretical investigations on flexural performance of hybrid fiber reinforced ECC-NC composite beams. *Case Studies in Construction Materials*, 20, 3178. doi:10.1016/j.cscm.2024.e03178.
- [37] Mandor, A., & El Refai, A. (2022). Strengthening the hogging and sagging regions in continuous beams with fiber-reinforced cementitious matrix (FRCM): Experimental and analytical investigations. *Construction and Building Materials*, 321, 126341. doi:10.1016/j.conbuildmat.2022.126341.
- [38] Khattak, N., Mansour, M., El-Maaddawy, T., & Ismail, N. (2022). Continuous Reinforced Concrete Beams Strengthened with Fabric-Reinforced Cementitious Matrix: Experimental Investigation and Numerical Simulation. *Buildings*, 12(1), 27. doi:10.3390/buildings12010027.
- [39] Feng, R., Liu, Y., Zhu, J. H., & Xing, F. (2020). Flexural behaviour of C-FRCM strengthened corroded RC continuous beams. *Composite Structures*, 245, 112200. doi:10.1016/j.compstruct.2020.112200.
- [40] Liu, D., Qin, F., Di, J., & Zhang, Z. (2023). Flexural behavior of reinforced concrete (RC) beams strengthened with carbon fiber reinforced polymer (CFRP) and ECC. *Case Studies in Construction Materials*, 19, 2270. doi:10.1016/j.cscm.2023.e02270.
- [41] Liu, L., Wang, L., & Xiao, Z. (2024). Flexural behavior of RC beams reinforced by ECC layer and steel plate: numerical simulation. *International Journal of Structural Integrity*, 15(3), 498–521. doi:10.1108/IJSI-08-2023-0083.
- [42] ASTM C39/C39M-20. (2021). Standard Test Method for Compressive Strength of Cylindrical Concrete Specimens. ASTM International, Pennsylvania, United States. doi:10.1520/C0039\_C0039M-20.
- [43] ASTM A770/A770M-03. (2010). Standard Specification for Through-Thickness Tension Testing of Steel Plates for Special Applications. ASTM International, Pennsylvania, United States. doi:10.1520/A0770\_A0770M-03.
- [44] ACI PRC-440.2-17. (2017). Guide for the design and construction of externally bonded FRP systems for strengthening concrete structures. American Concrete Institute, Michigan, United States.
- [45] Hanoon, A. N., Jaafar, M. S., Hejazi, F., & Abdul Aziz, F. N. A. (2017). Energy absorption evaluation of reinforced concrete beams under various loading rates based on particle swarm optimization technique. *Engineering Optimization*, 49(9), 1483–1501. doi:10.1080/0305215X.2016.1256729.
- [46] Mukhopadhyaya, P., Swamy, N., & Lynsdale, C. (1998). Optimizing Structural Response of Beams Strengthened with GFRP Plates. *Journal of Composites for Construction*, 2(2), 87–95. doi:10.1061/(asce)1090-0268(1998)2:2(87).
- [47] BS EN 1992-1-1:2004 (2004). Eurocode 2: Design of concrete structures - Part 1-1: General rules and rules for buildings. British Standards Institution, London, United Kingdom.
- [48] ACI 318-14. (1994). Building Code Requirements for Structural Concrete and Commentary. American Concrete Institute (ACI), Michigan, United States.
- [49] Aiello, M. A., Valente, L., & Rizzo, A. (2007). Moment redistribution in continuous reinforced concrete beams strengthened with carbon-fiber-reinforced polymer laminates. *Mechanics of Composite Materials*, 43(5), 453–466. doi:10.1007/s11029-007-0043-x.
- [50] Akbarzadeh, H., & Maghsoudi, A. A. (2010). Experimental and analytical investigation of reinforced high strength concrete continuous beams strengthened with fiber reinforced polymer. *Materials and Design*, 31(3), 1130–1147. doi:10.1016/j.matdes.2009.09.041.
- [51] El-Refaie, S. A., Ashour, A., & Garrity, S. W. (2003). Agging and Hogging Strengthening of Continuous Reinforced Concrete Beams Using Carbon Fiber-Reinforced Polymer Sheets. *ACI Structural Journal*, 100(4), 12653. doi:10.14359/12653.